Utah State University

DigitalCommons@USU

Space Dynamics Lab Publications

Space Dynamics Lab

2015

Particulate-Matter Emission Estimates from Agricultural Spring-Tillage Operations Using LIDAR and Inverse Modeling

Kori D. Moore
Space Dynamics Laboratory, North Logan, Utah

Michael D. Wojcik
Utah State University

Randal S. Martin
Utah State University

Christian C. Marchant
Utah State University

Derek S. Jones
Utah State University

William J. Bradford
Utah State University

Follow this and additional works at: https://digitalcommons.usu.edu/sdl_pubs

See next page for additional authors

Recommended Citation

Utah State University
MERRILL-CAZIER LIBRARY

Authors

Kori D. Moore, Michael D. Wojcik, Randal S. Martin, Christian C. Marchant, Derek S. Jones, William J. Bradford, Gail E. Bingham, Richard L. Pfeiffer, John H. Prueger, and Jerry L. Hatfield

Particulate-matter emission estimates from agricultural spring-tillage operations using LIDAR and inverse modeling

Kori D. Moore
Michael D. Wojcik
Randal S. Martin
Christian C. Marchant
Derek S. Jones
William J. Bradford
Gail E. Bingham
Richard L. Pfeiffer
John H. Prueger
Jerry L. Hatfield

SPIE.

Particulate-matter emission estimates from agricultural spring-tillage operations using LIDAR and inverse modeling

Kori D. Moore,[a,b,]* **Michael D. Wojcik,[a]** **Randal S. Martin,[b]**
Christian C. Marchant,[a,†] **Derek S. Jones,[a,‡]** **William J. Bradford,[a,‡]**
Gail E. Bingham,[a] **Richard L. Pfeiffer,[c]** **John H. Prueger,[c]** and
Jerry L. Hatfield[c]

[a]Utah State University Research Foundation, Space Dynamics Laboratory, 1695 North Research Park Way, North Logan, Utah 84341, United States
[b]Utah State University, Department of Civil and Environmental Engineering, 4110 Old Main Hill, Logan, Utah 84322, United States
[c]United States Department of Agriculture, National Laboratory for Agriculture and the Environment, Agricultural Research Service, 2110 University Boulevard, Ames, Iowa 50011, United States

Abstract. Particulate-matter (PM) emissions from a typical spring agricultural tillage sequence and a strip–till conservation tillage sequence in California's San Joaquin Valley were estimated to calculate the emissions control efficiency (η) of the strip–till conservation management practice (CMP). Filter-based PM samplers, PM-calibrated optical particle counters (OPCs), and a PM-calibrated light detection and ranging (LIDAR) system were used to monitored upwind and downwind PM concentrations during May and June 2008. Emission rates were estimated through inverse modeling coupled with the filter and OPC measurements and through applying a mass balance to the PM concentrations derived from LIDAR data. Sampling irregularities and errors prevented the estimation of emissions from 42% of the sample periods based on filter samples. OPC and LIDAR datasets were sufficiently complete to estimate emissions and the strip–till CMP η, which were ~90% for all size fractions in both datasets. Tillage time was also reduced by 84%. Calculated emissions for some operations were within the range of values found in published studies, while other estimates were significantly higher than literature values. The results demonstrate that both PM emissions and tillage time may be reduced by an order of magnitude through the use of a strip–till conservation tillage CMP when compared to spring tillage activities. © *The Authors. Published by SPIE under a Creative Commons Attribution 3.0 Unported License. Distribution or reproduction of this work in whole or in part requires full attribution of the original publication, including its DOI.* [DOI: 10.1117/1.JRS.9.096066]

1 Introduction

As aerosols have been shown to have detrimental effects on human health and visibility,[1] many governments have set regulations on allowable ambient concentrations. In the U.S., the Environmental Protection Agency (EPA) has established National Ambient Air Quality Standards (NAAQS) for particulate matter (PM) with aerodynamic equivalent diameters $\leq 10~\mu$m (PM_{10}) and PM with aerodynamic equivalent diameters $\leq 2.5~\mu$m ($PM_{2.5}$). If an area exceeds the

---

*Address all correspondence to: Kori D. Moore, E-mail: kori.moore@sdl.usu.edu

†Currently at National Geospatial-Intelligence Agency, 7500 Geoint Drive, Springfield, Virginia 22150, United States.

‡Currently at Campbell Scientific Inc., 815 West 1800 North, Logan, Utah 84321, United States.

NAAQS, the area's air-quality governing body is required to identify the causes and to restrict anthropogenic emissions in order to reduce PM levels below the standard.

The San Joaquin Valley of California, USA, was designated as noncompliant with the PM_{10} NAAQS in 1991 and given a "serious" classification in 1993.[2,3] Rule 4550, one of the regulations enacted by the San Joaquin Valley Air Pollution Control District (SJVAPCD) to reduce ambient PM_{10} levels in the San Joaquin Valley, required agricultural production operations to select several conservation management practices (CMPs) from a provided list, to submit their selections for SJVAPCD approval, and to implement approved CMPs. The CMPs were designed to reduce PM_{10} emissions from agricultural animal and crop production activities. However, the small amount of data available in the literature concerning the emissions' reductions from the CMPs for crop production tillage activities required that the control efficiency (η) of most tillage CMPs was estimated from emissions measurements of other operations.[4] The η of a CMP is the amount of particle emission reduction achieved relative to the conventional management practice. While the San Joaquin Valley Air Basin has since been classified as in attainment with the PM_{10} NAAQS, its maintenance plan requires that the same strategies employed to bring it back into attainment continue to be applied. In addition, other PM_{10} nonattainment areas such as Imperial Valley, California, and Phoenix, Arizona, have CMP or best management practice (BMP) rules in place for agricultural-tillage practices that are based on limited emissions measurements.

Previous agricultural-tillage PM emissions studies[5–12] have focused almost exclusively on measuring PM_{10} emission rates (ERs) and emission factors (EFs) from conventional tillage operations. For this discussion, EFs are emissions based on a quantity of production (e.g., $g \cdot m^{-2}$) and ERs are emissions that include a time factor (e.g., $g \cdot m^{-2} \cdot s^{-1}$). The California Air Resource Board (ARB) developed area source PM_{10} emission inventory calculation methodologies for agricultural tillage and harvesting operations based on the report by Ref. 5 (see Refs. 13, and 14). References 10 and 11 are the only instances of reporting PM emissions from standard tillage operations and a CMP (strip–till conservation tillage and combined operations, respectively). Reference 6 used elastic LIDAR (light detection and ranging) data collected during tillage emissions measurements to track plume movements in the downwind vertical plane and demonstrated plume depths were greater than the elevated point sensors located downwind at 10 m above ground level (agl). The report suggested the best method for sampling fugitive dust includes a combination of elastic LIDAR and strategically placed point samplers. Reference 11 used both filter-based mass concentration point samplers and a LIDAR system to monitor tillage emissions and estimated EFs from both datasets.

The study described in Ref. 11 was specifically initiated to provide more emissions η data with respect to a CMP in Rule 4550. The focus was on a typical fall tillage operation after a row crop harvest. A companion study funded by the San Joaquin Valleywide Air Pollution Study Agency was conducted to measure η of a spring tillage CMP using the same point sensor and LIDAR methodology. Research questions which this study was designed to address included: (1) what are the magnitude, flux, and transport of PM emissions produced by agricultural practices for row crops where tillage CMPs are being implemented versus, the magnitude, flux, and transport of PM emissions produced by agricultural practices where CMPs are not being implemented? (2) What are the values of η of equipment being used to implement the "combined operations" CMP? and (3) can these CMPs for a specific crop be quantitatively compared, controlling for soil type, soil moisture, and meteorological conditions? It is important to note that the main focus of this research was to quantify η of the selected CMP, which required the emissions to be quantified, and it was not an effort to provide representative EFs for any one of the agricultural operations involved. This paper summarizes the results of the PM measurements made during the field experiment, the calculated ERs, and addresses these research questions. A full report detailing all of the sampling methodology and results is given in Ref. 15.

2 Methodology

2.1 Site and Operation Description

This CMP η study was performed during the spring tillage sequence following the harvest of a winter wheat crop in preparation for the planting of corn. It was carried out in the San Joaquin

Valley of California during May and June 2008. Two adjacent fields were used with identical crop and flood irrigation treatments over the previous several years. Both fields were cultivated in winter wheat in late 2007 and were to be planted in corn for the 2008 summer growing season. The wheat was harvested while still green for silage 4 days before the tillage processes began, resulting in standing stubble but little plant material left on the surface. The site was chosen based on producer cooperation, historically dominant northwest winds, and field layout.

The surrounding landscape was topographically flat and dominated by agricultural production, including grain and corn fields, almond orchards, grape vineyards, and commercial dairy operations. Both fields were surrounded on all sides by roads. These roads, with the exception of one, were unpaved roads used for field access by farm machinery. The paved road, which was downwind of the fields during all measurements, was heavily traveled. Railroad tracks were located to the north of this site, with two to three trains passing by per day with varying numbers of cars. USDA NRCS soil survey data list the soil in both fields as soil type 130 – Kimberlina fine sandy loam, saline-alkali.[16]

The CMP selected for this study was the conservation tillage method. As described in Ref. 4, this CMP "involves using a system in which the soil is being tilled or cultivated to a lesser extent compared to a conventional system" and it is "intended to reduce primary soil disturbance operation such as plowing, disking, ripping, and chiseling." The conservation tillage CMP under study was a strip–till method which combines multiple operations to reduce the number of passes required and only disturbs the soil in strips 0.2 m wide centered every 0.8 m instead of disturbing the entire surface. Strip–till reduced both the number of passes and the tilled surface by about 75%, as well as left most of the wheat stubble still standing for ground cover. The strip–till implement used in this study was the Orthman 1-tRIPr. The cooperating farm had been using the Orthman 1-tRIPr for seedbed preparation on all of its fields for several years, with the exception of field 4, which was prepared by conventional tillage methods.

The conservation tillage CMP applied in this study consisted of three tillage activities totaling three operations across the field, excluding the building and removal of ditches. All three were monitored in separate sample periods. In comparison, the conventional tillage method as applied here had nine different tillage activities totaling 13 operations, excluding the building and removal of a ditch and field-edge borders. Monitoring of 12 of the operations occurred over nine sample periods. Note that not all operations were active throughout sample periods in which multiple operations occurred. Also, not all of the conventional tillage operations are intended to work the entire field, such as breaking down in-field borders. The term in-field borders as used here applies to low ridges of soil that separate the field into smaller areas for flood irrigation. The conventional tillage method was employed in field 4, shown in Fig. 1, and the conservation tillage CMP was used in field 5. The operations that were performed in each management practice are shown in order in Table 1, with their corresponding dates, equipment utilized, number of passes over a given area, tractor run time, total area worked, and sample period length. In cases where multiple tractors and implements were used within a sample period, they are listed in the order of use with the area worked and tractor time being summed. The lister, also called a double plow, prepares the soil for planting by creating furrows and ridges. The cultivator passes in the conventional tillage sequence function as mechanical weed control, whereas a chemical weed control (herbicide) is used in the CMP sequence.

During the first part of the lister operation, plant material not harvested along in-field borders caused clogging of the lister, decreasing effectiveness. A second tractor with a disk set was brought in to repeat the effort along the border lines to further reduce the size of residual plant material. Also note that the cultivator passes 1 and 2 and the roller pass for the first sample period on June 5 were not finished when planting in field 4 began and the second sample period was started. The combination of the cultivator and roller positions and meteorological conditions prevented significant impacts from these operations on downwind samples located near the southern end of the field.

Additionally, cultivator pass 4 was carried out the day after cultivator pass 3, but the emissions were not measured due to scheduling conflicts. It is assumed, in calculating the total PM emissions, that the ERs of both passes 3 and 4 were equal. In general, two cultivator passes are performed in sequence in opposite directions down the rows to ensure adequate weed control.
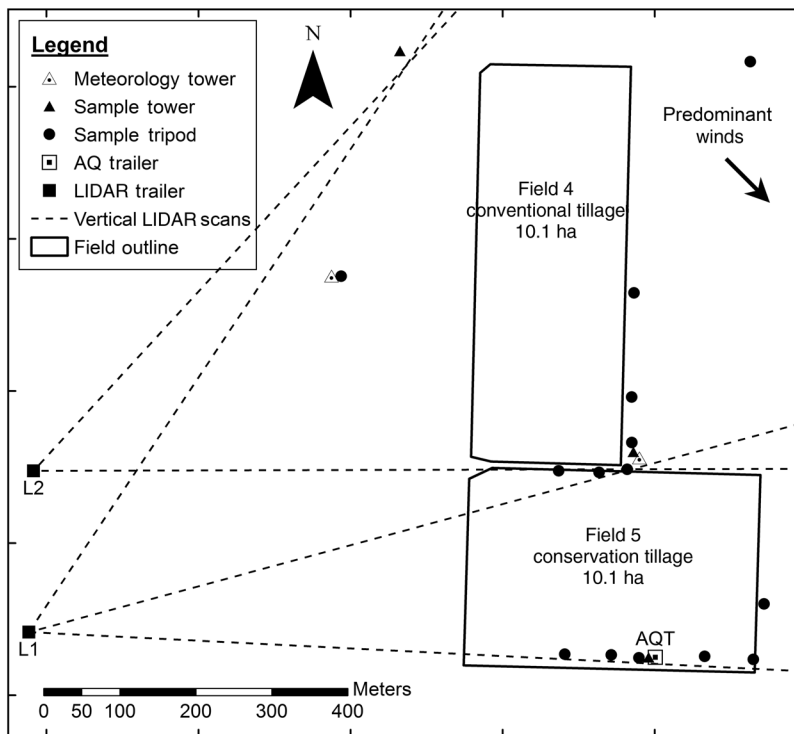
Fig. 1 Map of fields under study and the sample layout for each field. L1 and L2 represent light detection and ranging (LIDAR) locations used during sampling and dashed lines emanating from L1 and L2 show positions of vertical LIDAR scans.

Ditches and field-edge borders were built and then broken down in both fields between May 20 and June 5 to allow for flood irrigation prior to planting. Water for irrigation was taken from the earthen holding pond of the adjacent dairy; drainage ditches on the east side of both fields returned excess water to the same holding pond. As the ditch and field-edge border construction and removal were not measured in the CMP field, the corresponding step for the conventional tillage method was not considered in the total emissions per method. Prior to any spring tillage activities, both fields 4 and 5 had in-field borders running in roughly an east/west direction. The in-field borders in field 5 were not broken down and smoothed out, but instead were used for the summer corn crop. However, in field 4 they were removed and the irrigation water moved in the furrows created by the lister.

Field personnel observed operations continually and recorded notes on tractor operation times, potential contamination issues due to traffic on surrounding dirt roads and wind-blown dust, general meteorological observations, and so on.

2.2 Instrumentation and Sample Layout

A very dominant northwest wind was found in historical data for the months of May and June from a representative meteorological monitoring station in Stratford, California, in the California Irrigation Management Information System (CIMIS). Therefore, the PM and meteorology sampling layouts were configured to measure upwind conditions to the north and west and downwind conditions to the south and east.

Meteorological measurements were made at upwind and downwind locations with the instrumentation in Table 2. Vertical temperature, humidity, and wind speed profiles were measured using two 15.3 m towers, one upwind and one downwind as shown in Fig. 1. Each tower had five humidity/temperature sensors at 1.5, 2.5, 3.9, 6.2, and 9.7 m agl and 3-cup anemometers at 2.5, 3.9, 6.2, 9.7, and 15.3 m agl. Wind direction was measured at 15.3 m using a wind vane instead of the typical 10 m due to the fact that LIDAR measurements were made at higher elevations (up to 200 m agl) and the 15.3 m measurement height was reasoned to provide a better representation

Table 1 Information for each sample period regarding tillage operations, equipment used, tractor operation time, area worked and sample time.

Date	Tillage operation	Tractor make and model	Implement make and model	Number of passes	Sample time (hr)	Tractor time ($hr_{tractor}$)	Area worked (ha)	Tractor operation rate ($hr_{tractor}$/ha)
			Conservation tillage (field 5)					
May 17	Strip–till	Case MX255	Orthman 1-tRIPr, 6 row, 0.8 m spacing	1	3.92	3.05	9.1	0.34
June 7	Plant and Fertilize	Case MX255	Monosem twin-row planter model 6 × 2, 6 rows, 0.8 m spacing	1	5.33	3.82	9.1	0.42
June 11	Herbicide application	Kubota B-Series	Hardi ATV sprayer, 12.2 m boom	1	1.58	0.93	9.1	0.10
			Conventional tillage (field 4)					
May 17	Break down in-field irrigation borders	Case Puma 195	Custom border buster (2 sets of 3 disks that move soil from center to edges)	2, in-field border areas only	0.92	0.92	2.0	0.46
May 18	Chisel	Case MX255	Custom chisel, 4.0 m wide, 0.6 m depth, w/edged roller	1	6.58	6.18	8.5	0.73
May 19	Disk 1	Case Puma 195	International offset disk, 5.8 m wide, pulling a single axle (two smooth road tires), pulling a 5.8 m wide spiked roller	1	4.92	4.83	10.1	0.48
May 19	Disk 2	Case Puma 195	International offset disk, 5.8 m wide, pulling a single axle (2 smooth tires) pulling a 5.8 m wide spiked roller	1	5.25	4.73	10.1	0.47
May 20	Lister	Case MX255	Custom lister, 6 row, 1.0 m spacing	1	3.83	5.07	12.5	0.41
June 5	Break down ditch and field-edge borders, cultivator passes 1 and 2, and roller	Case Puma 195	International offset disk, 5.8 m wide	3, in-field border areas only				
		Kubota M8030DT	Custom 1-way disk (1 set of 3 disks that move soil from one side to the other)	8, east side edge only	7.25	7.43	23.9	0.31
		Case 870	Custom border buster (2 sets of 3 disks that move soil from center to edges)	4, east and west side edges only				
		Case Puma 195	Lilliston rolling cultivator, 6 rows wide, 1.0 m spacing	2				
		Case 2290	Flat roller, 6 rows wide	1				
June 5	Plant	Case Puma 195	Lilliston rolling cultivator, 6 rows wide, 1.0 m spacing	2	2.00	3.82	13.2	0.29
		Case 2290	Flat roller, 6 rows wide	1				
		John Deere 4055	John Deere MaxEmerge 2 row planter, single row, 6 rows wide, 1.0 m spacing	1				
June 18	Fertilize	Case 2290	Custom side-dress fertilizer, 6 rows wide, 1.0 m spacing, pulling a fertilizer tank (1 axle, 2 small smooth tractor tires)	1	2.17	1.08	3.8	0.28
June 25	Cultivator pass 3	Case 1370	Lilliston rolling cultivator, 6 rows wide, 1.0 m spacing	1	4.25	4.02	10.1	0.40

Table 2 Manufacturer, precision, and accuracy information for deployed meteorological instrumentation.

Instrument model	Manufacturer	Measured parameter	Accuracy
HMP45C	Vaisala, Oulu, Finland	Temperature	±0.2°C at 20°C
		Relative humidity	$\pm2\%$ for values in the range 0% to 90% and $\pm3\%$ for values in the range 90% to 100%
Gill 3-cup anemometer	RM Young Co., Traverse City, Michigan	Horizontal wind speed	±0.2 m s^{-1} over 1 m s^{-1}, threshold speed $= 0.5$ m s^{-1}
024A Wind Vane	Met One Instruments, Grants Pass, Oregon	Wind direction	±5 deg
Vantage Pro2 plus weather station	Davis Instruments, Inc., Hayward, California	Temperature	±0.5°C for values greater than -7°C, ±1.0°C for values less than -7°C
		Relative humidity	$\pm3\%$ for values 0% to 90% and $\pm4\%$ for values 90% to 100%
		Horizontal wind speed	±1 m s^{-1} or 5%, whichever is greater
		Wind direction	±3 deg
		Precipitation	$\pm3\%$ or 0.02 mm per event, whichever is greater
		Barometric pressure	±0.8 mm of mercury at 25°C
		Solar radiation	$\pm5\%$ of full scale
CSAT	Campbell Scientific, Inc., Logan, Utah	Three-dimensional wind vector	Offset error $< \pm8$ cm s^{-1} Gain error for wind vector within 20 deg of horizontal $< \pm6\%$ of reading
7500 Infrared Gas Analyzer	LI-COR, Lincoln, Nebraska	Gaseous H_2O and CO_2 concentrations	Dependent on calibration and environmental conditions

of both ground level and higher elevation wind direction than the 10-m height. Additionally, a meteorological station monitored wind speed, wind direction, temperature, relative humidity, precipitation, barometric pressure, and incoming solar radiation at 5 m agl at the air-quality trailer (AQT) location. Three pairs of three-dimensional sonic anemometers and infrared gas analyzers were deployed, one at an upwind location and one each downwind of the two fields of interest, to characterize upwind and downwind turbulences, as well as vertical fluxes of latent heat (evaporation), sensible heat, carbon dioxide, and horizontal momentum. Bulk density and soil moisture were quantified several times throughout the study, with calculations performed as described in Ref. 17.

PM mass concentrations were monitored by 20 MiniVol Portable Air Samplers (Models 4.2 and 5.0, AirMetrics, Eugene, Oregon), referred to hereafter as MiniVols. They are a portable, programmable, filter-based sampler that is battery-powered and yields an integrated sample over the exposure period. Filters were exposed for the duration of each sample period (see Table 1), yielding a single mass concentration measurement per sampler per sample period. Cumulative samples of particles up to $PM_{2.5}$ or PM_{10} are accomplished via an impactor plate assembly inserted just upstream of the filter; total suspended particulate-matter (TSP) may be sampled without an impactor assembly in place. The MiniVol impactor assembly is designed to operate a flow of 5.0 L $\cdot$ min^{-1}, though the flow rate is neither actively monitored nor actively controlled by the system. It is set prior to deployment by the user via a calibrated rotameter. Rotameter flow calibration was performed prior to deployment. While several studies have found that $PM_{2.5}$ and PM_{10} levels reported by MiniVols are very similar to concentrations measured by federal reference method (FRM, see 40 CFR 50.6 and 50.7) monitors, the slope of the particle removal

efficiency versus particle size curve of the MiniVol impactor assembly is less steep than required by FRM samplers.[18–21] Therefore, PM levels reported by the MiniVols should be considered as close approximations to those that would be given by FRM samplers.

Pre- and postweights for the 47 mm Teflon filters used to collect particles were quantified using a calibrated microbalance (Type MT5, Mettler-Toledo, Inc., Columbus, Ohio). Filter conditioning was carried out in accordance with guidance in 40 CFR 50 Appendix J. Sample period average mass concentrations were calculated by dividing the total mass catch (average postweight minus average preweight) by the volume of air sampled.

Particle size distribution (PSD) was measured by eight Aerosol Profilers (Model 9722, Met One Instruments, Grants Pass, Oregon), also known as optical particle counters (OPCs). The OPC sums particle counts in eight size bins over nominal 20-s sample periods. The particle diameters (d_p) for lower bin limits were 0.3, 0.5, 0.6, 1.0, 2.0, 2.5, 5.0, and 10.0 μm, with the last channel counting all particles $\geq$10.0 μm. The factory calibrations of signal strength versus particle size using polystyrene latex beads of known size were used due to varying atmospheric aerosol composition. The sample flows were not conditioned prior to passing through the sampling chamber during these measurements due to the dry conditions, though this is suggested in atmospheres with high relative humidity. OPC flow measurements and inter-OPC count calibrations were performed onsite and applied in postanalysis. Particle volume concentrations (V) per bin were calculated from the counts, assuming spherical particles and using the geometric mean diameter (GMD) as the representative d_p. Values of V in bins up to $d_p = k$ were summed to estimate the cumulative volume concentration (V_k).

The MiniVols and OPCs were deployed on towers and tripods upwind and downwind of the fields, as shown in Fig. 1. Most downwind sensors were moved between the downwind layouts, depending on the field being tilled. The AQT and the associated samplers did not move. The AQT is a 5 m $\times$ 2.5 m $\times$ 2.5 m cargo trailer used as the base of operations and equipped with tables, a refrigerator and dessicator for sample storage, and a rooftop platform for sensor deployment. Samplers were placed on tripods at 2 m agl at all locations except for those on top of the AQT at 5 m and those at the top of the towers at 9 m. Not all sample sites shown for a given setup were used in each sample period due to instrument availability limitations. However, samples were collected at a minimum of two upwind and six downwind locations during each sample period.

At most of the locations, multiple MiniVols with different impactor configurations and an OPC were collocated in order to characterize particle size and mass distributions. These data were used to calculate mass conversion factors (MCFs) for each size fraction (k), as described in detail by Ref. 21. In summary, the MCF_k is calculated using PM_k reported by MiniVols and V_k, averaged over the MiniVol sample time, from each sample location through the following equation:

$$\mathrm{MCF}_k = \frac{\mathrm{PM}_k}{V_k}, \tag{1}$$

where the units for PM_k are μg $\cdot$ m^{-3}, V_k are μm^3 $\cdot$ cm^{-3}, and MCF_k are g $\cdot$ cm^{-3}. Daily average MCFs were calculated across sampling locations.

The MCF is a simplified method to account for several complex and possibly interdependent variables that affect how an aerosol mixture is measured/detected based on both optical and aerodynamic properties. It incorporates many factors, such as particle shape, density, indices of refraction different from OPC calibration aerosols, and instrument sampling efficiencies, into a single scalar value. The MCF also includes effects due to optical systems measuring particles in ambient conditions while mass concentrations are calculated based on conditioned filters. This effect may be significant in humid environments, but the effect is assumed to be negligible in warm and dry conditions such as those found during this study. The MCF_k values were used to convert the OPC V_k into PM_k to examine concentrations on a much finer temporal scale than possible with the filter data.

The Aglite LIDAR system was deployed to characterize PM concentrations in addition to point sensors. The Aglite LIDAR is a portable system using a micropulsed Nd:YAG laser with three wavelengths (λ), 355, 532, and 1064 nm. It has the capability to scan 280 deg in azimuth

and from -10 deg to $+45$ deg in elevation. The effective range is 500 m to 15 km with each range bin approximately 6 m in length.[22] The LIDAR was placed in crosswind positions 550 m from the nearest tillage area border. It was at L1, as shown in Fig. 1, from May 17 through June 11 and at L2 for the June 18 sample period. Critical component failures prevented its use for the June 25 sample period.

The LIDAR continuously performed vertical scans on the upwind and downwind sides of the field, horizontal scans over the field, and calibration stares throughout tillage observation periods. Lines of approximate vertical scan locations are shown in Fig. 1 by the dashed lines emanating from L1 and L2; horizontal scans moved between upwind and downwind vertical scan positions at 0.75 deg from horizontal. Vertical scans started at 0.75 deg and extended up to between 15 deg and 45 deg. The maximum vertical angle varied between sample periods but was usually ≤ 25 deg. Images resulting from vertical scans were monitored throughout each sample period to ensure that the maximum vertical extent of the plumes was entirely captured; modifications to the maximum vertical extent were made as needed. The LIDAR beam was about 10 m agl at the closest edge of the fields at 0.75 deg in elevation. The beam was kept at or above this level due to eye safety concerns. The LIDAR system did not measure plumes below this level and, therefore, may underestimate PM flux.

A calibration stare refers to short periods (60 to 120 s) when the LIDAR beam is held adjacent to an upwind tower with collocated point sensors. Calibration stares were routinely performed throughout the sample period at 10 to 20 min intervals. In postprocessing, LIDAR return signals collected during calibration stares were calibrated to PSD and V_k measurements. The process used to accomplish this is described in detail by Refs. 23 and 24 and will now be summarized. The calibration process is illustrated in Fig. 2 and was carried out through the following steps:

1. The raw LIDAR signal was preprocessed to yield range (R) and background corrected return power with R.
2. Relationships between backscatter (β), extinction (α), and V_k of the aerosol components were established based on OPC data from both upwind and downwind locations. The PSD of both the background and plume aerosol as a function of time was calculated, after which the α and β coefficients at the calibration range (R_c) at each LIDAR λ were calculated using Mie scattering theory applied to the PSDs. Assumptions made in these calculations were (1) all particles were spherical and (2) the bulk aerosol had a complex index of refraction equivalent to a mineral particle type (1.53–0.008i; Ref. 25).
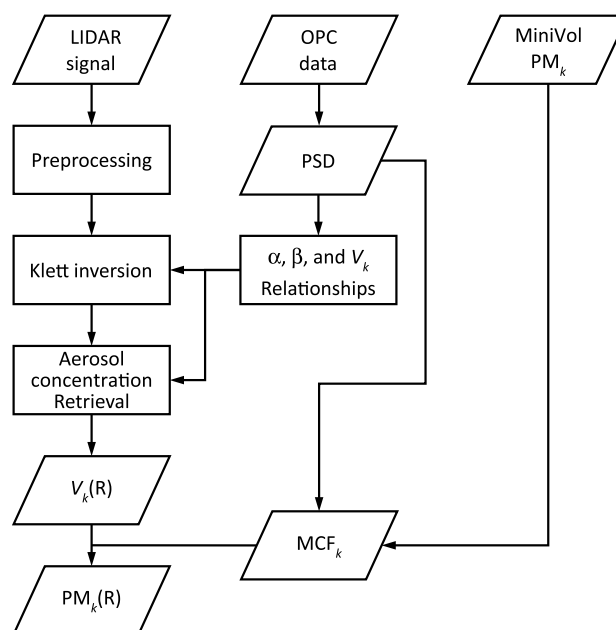

Fig. 2 Process diagram for LIDAR PM calibration algorithm.

3. The inversion of the LIDAR data was performed using a form of Klett's solution[26] for two scatterers where α is proportional to β using the relationships found in step 2, resulting in α and β as function of R and λ [$\alpha(R, \lambda)$, $\beta(R, \lambda)$]. The backward integration Klett method was applied to $R < R_c$ and the forward integration method was used for $R > R_c$. The backward integration method yields more stable solutions than the forward integration method and is, therefore, preferred. The calibration point R_c was placed at the farthest range possible within property ownership/field of view limitations to maximize the extent of the range of interest subject to backward integration.
4. The relationships from step 2 were used to convert $\beta(R, \lambda)$ into $V_k(R)$ through a least-squares method in the aerosol concentration retrieval step.
5. Conversion from $V_k(R)$ to $PM_k(R)$ was accomplished through the use of MCF_k.

This calibration method allows a scanning LIDAR to estimate PM_k concentrations surrounding an area/source of interest at a much finer spatial scale than possible with point sensors.

2.3 Emission Calculation Methods

The PM_k data from the point sensors and LIDAR were used to the estimate η of the conservation tillage CMP in this study. The point sensor PM_k concentrations were coupled with an air dispersion model through inverse modeling. In typical air dispersion model applications, a source ER is supplied to a model which then calculates the resulting concentration (C_{sim}) at a given receptor location. Inverse modeling involves using a dispersion model and concentrations measurements around a source activity ($C_{downwind}$, C_{upwind}) in order to estimate the observed ER (Q_{meas}). An initial ER (Q_{sim}) is supplied to the model to calculate C_{sim}, then the following equation is used to calculate Q_{meas}:

$$Q_{meas} = \frac{C_{downwind} - C_{upwind}}{(C/Q)_{sim}}. \tag{2}$$

If the model used has a proportionally linear response in C_{sim} to changes in Q_{sim}, the ratio $(C/Q)_{sim}$ is a scalar value independent of the given Q_{sim} value, i.e., there are no local maxima or minima that might influence the resulting value of Q_{meas}.

AERMOD (American Meteorological Society and U.S. EPA Regulatory Model), a Gaussian air dispersion model that estimates C_{sim} at a given receptor point based on meteorological conditions, source strength, and the horizontal and vertical distances of the receptor from the source, was selected to perform the inverse modeling estimation of Q_{meas}.[27] It is an air dispersion model currently recommended for regulatory modeling by the U.S. EPA. It operates in 1 h time steps, has a proportionally linear response in C_{sim} to changes in Q_{sim}, and assumes steady-state conditions, continuous emissions during a time step, conservation of mass, and C_{sim} resulting from multiple sources are additive. Pollutant distribution is modeled as Gaussian in the stable boundary layer in both the horizontal and vertical directions. In the convective boundary layer, horizontal dispersion is modeled as Gaussian while vertical pollutant distribution is modeled as bi-Gaussian. The spatial resolution of C_{sim} is controlled by the user through discrete and/or gridded receptor points. The commercially available user-interface AERMOD View from Lakes Environmental, Inc. (Waterloo, Ontario, Canada), with AERMOD version 13350, was employed.

Onsite measured wind speed, wind direction, temperature, humidity, and solar radiation were used by AERMET, the meteorological preprocessor for AERMOD, to create both surface and elevated meteorological input files. Wind, temperature, and humidity data were used from the upwind meteorology tower dataset, with wind speed from 9.7 m agl and temperature and relative humidity from 2.5 m agl. Incoming solar radiation was measured at the AQT location. Percent cloud cover was set to zero based on visual observations during the measurement periods.

The land-use classification on all sides of the site was cultivated land. Values provided to AERMET for midday albedo and Bowen ratio of 0.18 and 1.5, respectively, were suggested as average summer values under dry conditions for a fallow agricultural field in Ref. 28. The surface roughness length (z_0), also required by AERMET, was calculated based on wind profile measurements at the upwind meteorological tower using the following equation which relates

wind speeds (u_1, u_2 in m $\cdot$ s^{-1}) at two heights (z_1, z_2 in m) and was derived from the integrated logarithmic wind speed profile equation:

$$\frac{u_2}{u_1} = \frac{\ln\left(\frac{z_2}{z_0}\right)}{\ln\left(\frac{z_1}{z_0}\right)}. \tag{3}$$

A least sum of squares of residuals methodology was used to determine the value of z_0 that best fit measured wind speeds at the higher elevation of two paired wind speed time series over the study period. A z_0 value of 0.02 m was calculated as the arithmetic average of the values that best fit six pairings of wind speeds measured at 2.5, 3.9, 6.2, and 9.7 m agl, i.e., 2.5 and 3.9 m, 2.5 and 6.2 m, 2.5 and 9.7 m, 3.9 and 6.2 m, 3.9 and 9.7 m, and 6.2 and 9.7 m. The cup anemometer at 15.3 m malfunctioned during this deployment, rendering the data unusable for this analysis. The upwind location was selected for this analysis as the downwind tower was removed on June 12 to support another study nearby. The AQT was also removed from the southern edge of field 5 at the same time.

Tillage operations were modeled as ground level area sources with initial plume heights of 0 m and areal extents equal to the actual tilled portions of the field. Most operations covered all or most of the fields within a sample period, but some, such as the break down in-field borders operation, were intended to only work a small portion of the field surface. Tilled areas and sampler locations were measured using a hand-held GPS unit. The Q_{sim} values for each modeled operation were based on a preliminary average ER value across all tillage operations from Ref. [11] of 8.6 μg $\cdot$ s^{-1} $\cdot$ m^{-2} per operation per pass multiplied by the number of passes over the field within a sample period. Sources were activated or deactivated in hourly time steps throughout a simulated sample period according to the tractor operation times as monitored by onsite personnel. Discrete receptors were set at each sampling location to yield C_{sim} for inverse modeling comparisons. Uniform Cartesian receptor grids at 2 m agl and 15 m spacing between points were set from upwind sampling locations to several hundred meters downwind of the fields to visualize predicted plume movement, shape, and concentration. Hourly C_{sim} values were averaged over the modeled sample period. Modeled plume edge effects were avoided by eliminating those locations with C_{sim} less than 10% of the maximum C_{sim}, adapted from suggestions by Ref. [29], from emissions calculations.

The second ER and EF calculation approach was a mass balance applied to the LIDAR PM$_k$ data. Assuming uniform background aerosol levels, average upwind concentrations were subtracted from concentrations in and around detected plumes in the downwind vertical scans. The difference was multiplied by the component of the wind perpendicular to the beam to calculate the horizontal flux of PM through the downwind vertical scanning plane. Fluxes were summed across the vertical plane, averaged over the length of the sample period, and then divided by the size of the tilled area to calculate the mean EF of PM$_k$ from the field surface. The EF was further divided by the total tractor time to calculate the mean ER of each operation. This method of calculating ERs and EFs using LIDAR is described in detail in Ref. [30].

Vertical profiles of PM mass concentration, horizontal wind speed, and wind direction are required to use the mass balance approach. The PM profile was provided by the LIDAR PM$_k$ data. Profiles of wind speed were calculated using the wind speed power law, as given by Ref. [31],

$$u_2 = u_1\left(\frac{z_2}{z_1}\right)^p, \tag{4}$$

where z_1 and z_2 are the lower and upper elevations (m), respectively, p is a dimensionless number that varies with atmospheric stability, and u_1, u_2, z_1, and z_2 have been previously defined. Ref. [31] lists $p \approx 0.5$ for very stable conditions and $p \approx 0.15$ for very unstable conditions. The horizontal wind speeds recorded at the upwind tower were used to find the values of p that best fit the time series of measured profiles up to 9.7 m agl, with imposed minimum and maximum limits of 0.1 and 0.6, respectively. Derived values of p across all sample periods ranged from 0.10 to 0.60 and averaged 0.19. These p values were then combined with the minute-averaged

wind speeds in the wind speed power law to calculate the vertical profile of horizontal wind speed up to 250 m agl, though most sample periods did not require data more than 150 m agl.

Wind direction over the vertical profile was assumed to be constant. Though wind direction is known to change in a vertical profile, the influencing factors may be complex and the magnitude and direction of change highly variable. Therefore, in the absence of measured data, the assumption that wind direction did not change with increasing elevation over the 250 m profile was used.

3 Results and Discussion

Results of the soil analyses were almost identical between the two fields, suggesting little to no difference in the influence of soil properties on airborne PM emissions. Bulk densities averaged 1.57 ± 0.05 g · cm^{-3} for field 4 and 1.57 ± 0.08 g · cm^{-3} for field 5. Unless otherwise noted, error values represent one standard deviation (σ). Average soil moisture values in both fields measured immediately prior to May sample periods varied between 1.0% and 3.3%, showing very little change across operations. However, average soil moisture measured on June 5 in field 4 was 6.1% and 8.2% in field 5 on June 7. This increase was likely due to flood irrigation in both fields shortly after the May 20 sample period. A precipitation event occurred shortly after irrigation, but the quantity was not measured and the effect was assumed to be masked by the flood irrigation.

Wind conditions were favorable for the designed sampling layouts throughout the study period, as shown in Fig. 3 and Table 3. The median, minimum, and maximum values for sample period average winds were 4.0, 1.9, and 5.6 m · s^{-1}, respectively, for speed and 321 deg, 315 deg, and 335 deg, respectively, for direction. Sample periods were generally hot and dry, with median, minimum, and maximum sample periods average temperatures and relative humidity values of 31.4 ℃, 24.7 ℃, and 36.8 ℃ and 27%, 16%, and 40%, respectively.

3.1 Particulate-Matter Concentration Measurements

A total of 296 filter samples were collected: 116 PM$_{2.5}$ (39%), 116 PM$_{10}$ (39%), and 64 TSP (22%). Calculated PM$_{2.5}$ concentrations based on filter catch ranged from 23.2 to 3244.9 μg · m^{-3};
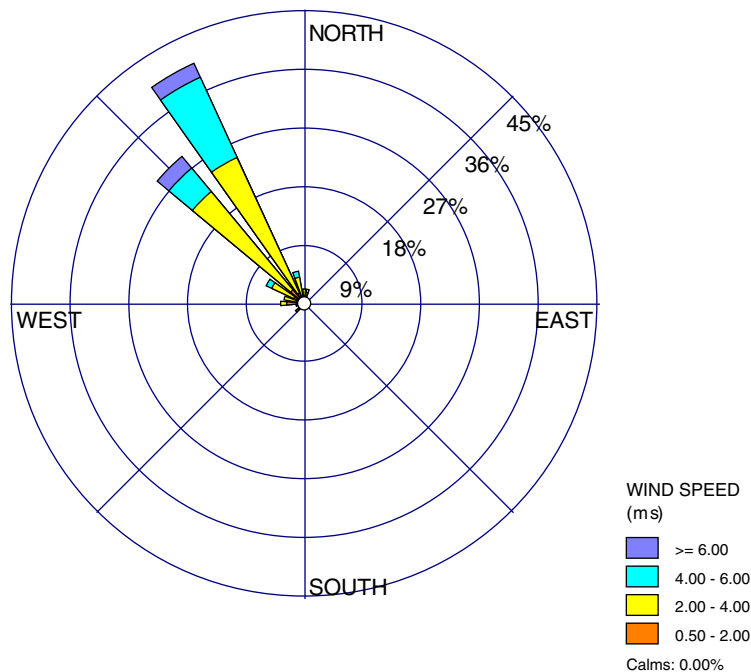

Fig. 3 Wind rose for the hourly averaged wind observations during the days on which samples were collected.

Table 3 Period-averaged meteorological measurements $\pm 1\sigma$ made at the upwind meteorological tower. Temperature, relative humidity, and wind speed were measured at 9.7 m agl and wind direction was measured at 15.3 m agl.

Date	Operation, field	Ambient temperature (°C)	Relative humidity (%)	Wind speed (m s^{-1})	Wind direction (deg)
May 17	Strip–till, field 5	32.3 ± 2.1	33 ± 4	3.6 ± 0.6	321 ± 15
May 17	Break down in-field borders, field 4	36.8 ± 0.2	24 ± 0.3	4.3 ± 0.6	321 ± 8
May 18	Chisel, field 4	33.8 ± 2.8	29 ± 4	4.3 ± 1.2	325 ± 16
May 19	Disk 1, field 4	31.4 ± 2.5	27 ± 3	2.9 ± 0.8	318 ± 22
May 19	Disk 2, field 4	35.3 ± 1.5	21 ± 3	3.3 ± 0.5	319 ± 16
May 20	Lister, field 4	29.1 ± 2.2	30 ± 10	5.1 ± 1.1	320 ± 10
June 5	Break down ditch, cultivators 1 and 2, and roller, field 4	24.7 ± 2.6	34 ± 7	3.3 ± 1.3	320 ± 30
June 5	Plant, field 4	27.6 ± 0.5	26 ± 2	4.0 ± 0.9	315 ± 7
June 7	Plant and fertilize, field 5	22.5 ± 2.7	40 ± 9	4.0 ± 1.0	335 ± 20
June 11[a]	Herbicide, field 5	29.1 ± 0.1	19 ± 1	3.8 ± 0.6	326 ± 17
June 18	Fertilize, field 4	34.1 ± 0.3[a]	16 ± 1[a]	5.6 ± 0.7	326 ± 4
June 25[a]	Cultivator 3	30.2 ± 2.5	29 ± 5	1.9 ± 0.8	328 ± 29

[a]Data taken from downwind tower due to missing data at upwind tower.

PM_{10} concentrations ranged from 38.1 to 1458.4 $\mu g \cdot m^{-3}$; TSP concentrations ranged from 73.6 to 2276.9 $\mu g \cdot m^{-3}$. The average method detection limit (MDL, $n = 13$), calculated based on sample period duration, the targeted flow of 5.0 L $\cdot min^{-1}$, and the minimum detectable difference between pre- and post-test filter weights of 5 μg, was 6.6 ± 4.9 $\mu g \cdot m^{-3}$ and the median was 4.3 $\mu g \cdot m^{-3}$, with a range of 2.3 $\mu g \cdot m^{-3}$ for a run length of 7.3 h to 17.3 $\mu g \cdot m^{-3}$ for a run length of 1.0 h.

Of the 296 filter samples collected, 98 (33%) did not pass quality analysis (QA) checks applied to the dataset. QA checks included visual inspection of filter surfaces, sample log inspection for noted problems, OPC time series examination for contamination (used mostly at upwind sites), concentration consistency across sampling locations, and concentration comparisons among $PM_{2.5}$, PM_{10}, and TSP at each sample location. In-depth descriptions of the QA checks are found in Ref. 15. An investigation into the cause(s) of this high rate of failure was conducted and a summary of conclusions is provided in the following paragraph. A large number of failures of near-source, downwind samples relative to the total number of downwind samples collected were found in the sample periods from May 18 to May 20. This, when combined with the results from the investigation into the large number of failures, casts doubt on the validity of the remaining near-source downwind samples from those runs. Therefore, all near-source downwind MiniVol samples for these sample periods were removed from MCF and ER calculations, rendering the upwind and far-source downwind samples that passed QA unusable for estimating PM emissions. The filter dataset used to calculate ERs and EFs totaled 131 samples (44%). Concentration ranges for this dataset were 26.7 to 149.8 $\mu g \cdot m^{-3}$ for $PM_{2.5}$, 47.4 to 489.4 $\mu g \cdot m^{-3}$ for PM_{10}, and 102.9 to 1,896.9 $\mu g \cdot m^{-3}$ for TSP. The size fraction distribution of filters used to estimate emissions was nearly identical to the total sample set: 51 (39%) were $PM_{2.5}$, 50 (38%) were PM_{10}, and 30 (23%) were TSP.

Filters that did not pass QA were found to have been contaminated during one or more of the following stages: sampling, filter handling, and filter storage. Evidence of "particle bounce" was found on many $PM_{2.5}$ and PM_{10} samples collected during May sample periods. Particle bounce occurs when particles that collide with the impactor plate are re-entrained in the airstream and

collected on the filter downstream and result in higher reported levels than actually existed. This issue is most likely due to exposing the MiniVol samplers to dust plumes exceeding the maximum recommended exposure level and improper instrument maintenance and cleaning through the May sample periods. Corrective action in the form of inspection after each deployment and cleaning, if needed, was taken during the June sample periods; no issues associated with particle bounce were observed in the second portion of the study. Additionally, some particles were observed on top of and imbedded into the plastic annular ring around the Teflon filter material—the plastic ring is covered by the filter holder assembly during deployment. This was likely due to contamination during onsite filter storage or handling. Efforts were made to minimize this issue throughout, especially during the June sample periods. However, wind-blown dust did impact the handling and storage area on May 20.

The collected OPC data were used to calculate PSD, V, and V_k values. Unlike the downwind MiniVol samplers, the downwind OPCs were not overwhelmed by the dust plumes from the tillage activities—the manufacturer specified range of the OPC of 0 to 3.18×10^8 particles m^{-3} was never exceeded—and thus provided usable data throughout all sample periods. Background and downwind PSD and V profiles varied throughout the study, as shown in Fig. 4. The particle concentrations in this figure were calculated as the change in number (N) per change in natural logarithm of d_p ($dN/d[\ln(d_p)]$) where d_p is the GMD per bin. The particles emitted by the tillage activities were generally large ($d_p > 5$ μm) and, therefore, strongly dominated the volume and mass contributions of the activity to near-source atmospheric particle loadings. Three to four OPCs were in positions immediately downwind of the field under study in each sample period, with between one and four OPCs in upwind locations.

OPC time series data at upwind locations were examined for contamination from upwind activities, such as unpaved road traffic. Contamination was found in six of the 12 sample periods, with five of those occurring at the sample site adjacent to the upwind meteorological tower and immediately downwind of an unpaved road. Large, short-duration spikes indicative of contamination were removed from the upwind data in these instances to estimate the background aerosol concentration. In each instance this was performed, the estimated background levels were in very good agreement with those measured by an OPC at a different, uncontaminated upwind location.
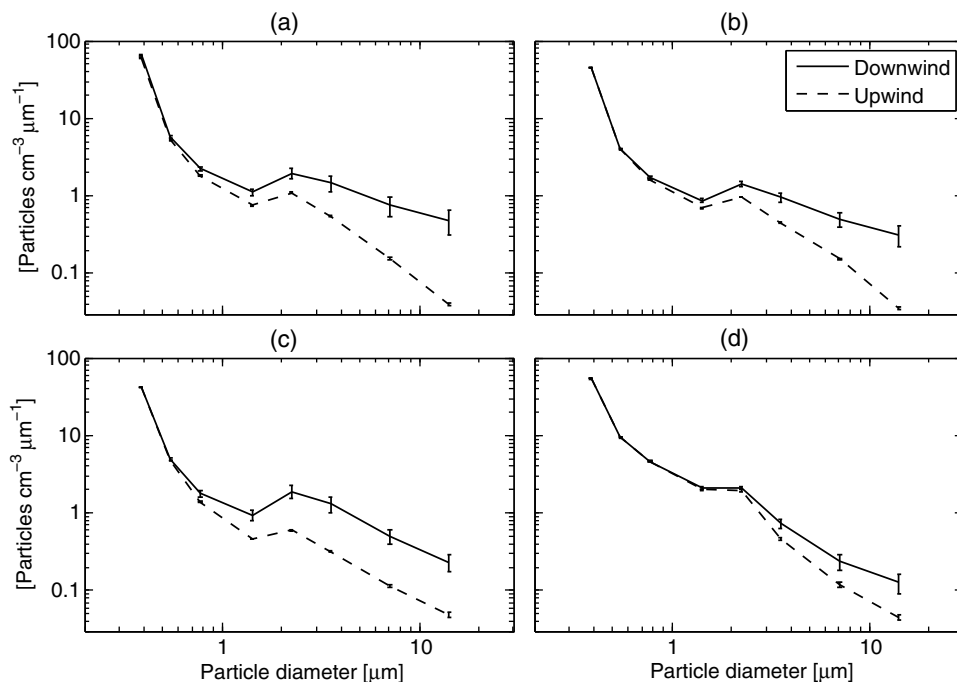

Fig. 4 Sample period-averaged upwind and downwind particle size distributions (PSDs) as measured by optical particle counters (OPCs) for (a) May 17, strip–till operation, field 5, (b) May 18, chisel operation, field 4, (c) June 5, plant operation, field 4, and (d) June 7, plant and fertilize operation, field 5. Error bars represent the 95% confidence intervals about the average.

Filter samples collected at upwind locations with contamination indicated by OPC data were removed from ER estimation.

Those filter samples that passed QA, including the upwind and far-source downwind samples from May 18 to May 20, were used to estimate MCF_k values if collected adjacent to an OPC. Most of the daily average MCF_{10} and MCF_{TSP} values were within the expected range of 1 to 3 $g \cdot cm^{-3}$. However, the daily average $MCF_{2.5}$ values were much larger than expected, with individual values ranging from 3.2 to 28.2 $g \cdot cm^{-3}$, having a mean of 14.6 ± 3.7 $g \cdot cm^{-3}$ and a median of 10.1 $g \cdot cm^{-3}$. For comparison, the densities of pure nickel and mercury are 8.9 and 13.5 $g \cdot cm^{-3}$, respectively. In past field campaigns, $MCF_{2.5}$ has generally been higher than MCF_{10} and MCF_{TSP} values, but these $MCF_{2.5}$ values were much higher than those seen before and account for the majority of values above 5 $g \cdot cm^{-3}$ reported in Ref. 21. Due to the nonphysically large numbers, the calculated $MCF_{2.5}$ was not used. Instead, the average soil density of 2.65 $g \cdot cm^{-3}$ given in the USDA NRCS National Soil Survey Handbook was used as a constant $MCF_{2.5}$ for all sample periods.[32] Using a constant $MCF_{2.5}$ may affect the accuracy of calculated $PM_{2.5}$ concentrations, ERs, and EFs and the value of $\eta_{2.5}$. However, as will be shown later, the effect on $\eta_{2.5}$ was assumed to be small as the values were very close to those of η_{10} and η_{TSP}. Table 4 presents the daily MCF_k values used to convert V_k calculated from LIDAR and OPC measurements to PM_k.

The cause of the high $MCF_{2.5}$ values is unknown. No significant differences in $PM_{2.5}$ chemical composition were observed between sample periods with higher and lower $MCF_{2.5}$ values. While PSDs varied between sample periods, no trends in PSDs sufficient to explain high/low $MCF_{2.5}$ groupings were observed. Higher average $MCF_{2.5}$ values were not restricted to sample periods in which evidence of particle bounce was found (May 18 to May 20); those filters exhibiting evidence of particle bounce were removed prior to MCF calculations. MCF_{10} and MCF_{TSP} patterns tended to follow $MCF_{2.5}$ patterns, having correlation coefficients (r) of 0.64 and 0.84, respectively, but with much smaller changes in amplitude. Good negative correlations ($-0.69 \leq r \leq -0.64$) were found when comparing all MCF_k values with sample duration. This means that MCF_k tended to increase as sample duration decreased.

One potential explanation consistent with these relationships is contamination during filter handling and storage. If filters were equally contaminated, the greatest effect would be found on

Table 4 Mass conversion factors (MCFs) used to convert optical particle measurements to mass concentrations for each sample day and averaged for the whole campaign. Error values represent the 95% confidence interval for $n \geq 3$. A constant $MCF_{2.5}$ value equal to the average density of soil was used due to nonphysically high values calculated for most of the sample days.[32]

Date	$MCF_{2.5}$		MCF_{10}		MCF_{TSP}	
	Average	n	Average $\pm$ 95%CI	n	Average $\pm$ 95%CI	n
	$(g \cdot cm^{-3})$	Count	$(g \cdot cm^{-3})$	Count	$(g \cdot cm^{-3})$	Count
May 17	2.65	—	2.6 ± 1.3	9	4.4 ± 4.0	7
May 18	2.65	—	1.6	2	1.6 ± 0.1	3
May 19	2.65	—	1.7 ± 0.3	5	1.6 ± 0.3	8
May 20	2.65	—	1.6 ± 0.5	5	1.4 ± 0.2	4
June 5	2.65	—	1.8 ± 0.3	5	1.5	2
June 7	2.65	—	1.5 ± 0.3	5	1.4 ± 0.2	4
June 11	2.65	—	4.3 ± 1.2	4	2.9 ± 0.5	4
June 18	2.65	—	1.8 ± 0.5	6	2.3 ± 1.0	4
June 25	2.65	—	2.0 ± 0.3	6	2.2 ± 0.6	5
Average	—	—	**2.1 ± 0.3**	**49**	**2.3 ± 0.7**	**44**

those samples with the smallest mass catch, i.e., samplers with $PM_{2.5}$ impactor configurations or shorter sample times. Unfortunately, field and lab blanks were not collected to monitor for and quantify such contamination; this oversight has been corrected in subsequent studies.

An alternate contamination test is a comparison with independent and proximate PM measurements, though conclusions from this test are limited by comparability of sample characteristics. The closest independent monitoring site was a suburban monitoring station operated by the SJVAPCD, which reported 24-h average PM_{10} concentrations on 3 days during which tillage monitoring occurred. The SJVAPCD 24-h average PM_{10} and study site mean background PM_{10} pairs were, respectively, 38 and 38 $\mu g \cdot m^{-3}$ for May 18, 34 and 47 $\mu g \cdot m^{-3}$ for June 5, and 38 and 163 $\mu g \cdot m^{-3}$ on June 11. Differences in sample period (24-h versus 1.5-h to 7.5-h and limited to daylight hours only), location setting and local sources (suburban versus rural), and instrumentation (FRM versus MiniVol) existed between the two datasets and contributed to observed differences. The differences in concentration between the two sites on May 18 and June 5 were within the range of expected values and do not support the sample contamination hypothesis. At first glance, the large difference on June 11 may be interpreted to support this hypothesis. However, all filters collected during this sample period easily passed the visual filter inspection for particle bounce and particles on and/embedded into the annular ring. If filter contamination did occur during this field study, it does not appear to have been consistent based on the comparison with proximate PM_{10} measurements nor evident in the applied QA tests. Therefore, the cause of the high $MCF_{2.5}$ values is unknown and no further data exclusions were made.

Sample period-averaged OPC PM_k data were ranged from 4.3 to 60.2 $\mu g \cdot m^{-3}$ for $PM_{2.5}$, 41.2 to 641.1 $\mu g \cdot m^{-3}$ for PM_{10}, and 95.3 to 3,271.9 $\mu g \cdot m^{-3}$ for TSP. OPC PM_k values at the native 20-s averaging period had much higher ranges across all k as the plumes emitted by the roving tillage activities impacted the point samplers in short bursts, the impact of which was reduced when averaged with intervals measuring lower levels. LIDAR-derived PM_k also had a high variability for the same reason. This is evident in Fig. 5, which presents PM_{10} reported by all three systems at 9 m agl at the downwind tower for the June 18 sample period (14:00–16:10). The dashed black line represents the sample period average PM_{10} value based on the MiniVol filter sample, the red line represents the PM_{10} based on 20 s OPC data, and the blue markers represent the LIDAR-derived PM_{10} for each 0.5-s signal averaging period. The higher temporal sampling frequency of the optical systems shows the timing and magnitude of individual plumes impacting the collocated group not resolved by the single MiniVol sample. The LIDAR beam was not continuously adjacent to the point sensors as it was performing upwind calibration stares and downwind vertical scans, leading to the gaps seen in the LIDAR time series. The LIDAR reported elevated PM_{10} levels when collocated during plume impaction
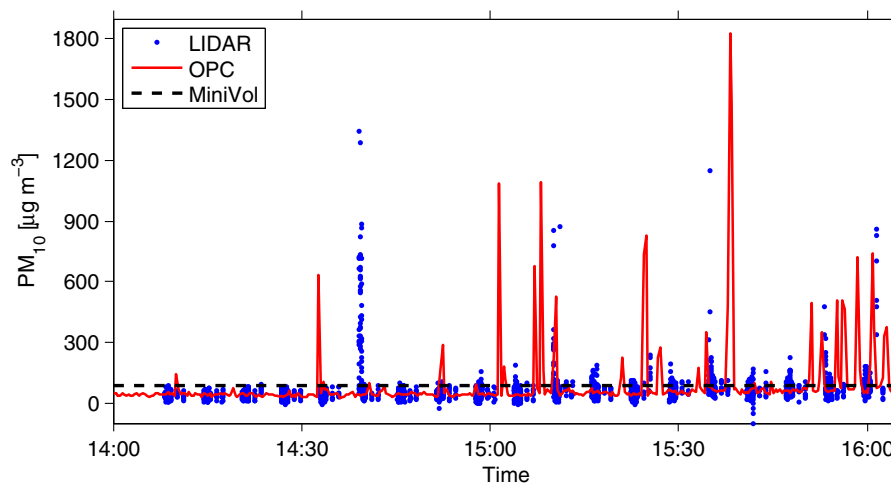

Fig. 5 Time series of PM_{10} concentrations as reported by the collocated OPC, MiniVol filter sampler, and LIDAR at 9 m agl on the downwind side of the tillage activity for the June 18 sample period (14:00–16:10).

events. It also reported elevated levels when the point sensors did not—this was due to part of a plume being within the 6 m long LIDAR bin but not significantly impacting the tower. Negative PM_k values were occasionally reported by the LIDAR, as seen here. These were artifacts of the optimization in the calibration procedure and are not real—negative PM concentrations are not possible.

While the scanning LIDAR was at a disadvantage compared to the point sensors in monitoring PM continuously at a given location in Fig. 5, a significant advantage of the LIDAR over the point sensors is its ability to monitor plumes over a line or area. For instance, the data shown in Fig. 6 were collected in a stare adjacent to the downwind tower (location indicated by the solid black line at constant range) over approximately 1 min of the sample period in Fig. 5. The LIDAR detected multiple, highly concentrated plumes at varying distances, only one of which appears to impact the tower. The bottom plot shows the average PM_{10} concentration with range during this time.

The vertical scanning profiles used to monitor plumes emitted by the tillage activities allowed measurement of vertical and along-beam horizontal plume extents. Monitored plumes reached elevations up to 150 m agl at the downwind LIDAR scanning plane, though most remained below 100 m. Plume widths also varied. Figure 7 provides an example of two plumes captured in a single vertical scan on June 5 when two different tillage operations were performed in different areas of the field. The plume closer to the LIDAR is lower and denser than the plume farther away.

Comparisons between PM_k concentrations from MiniVol, OPC, and LIDAR data at upwind and downwind locations were performed for each sample period as a check on the use of the MCF_k and the LIDAR calibration procedure. Accurate estimates of PM_k are necessary for accurate estimates of PM emissions. The MiniVol, as it measures PM_k directly at each point, is assumed to be more representative of the actual PM_k than the OPC and LIDAR. Most inter-instrument comparisons revealed upwind values agreed fairly well, but greater differences were found in comparisons at downwind sample sites. Potential reasons for the similarities and differences at both upwind and downwind point sampler locations will be discussed in the following paragraphs, with an example comparison provided as well.

The similarity of PM_k estimated by the OPC and LIDAR at the upwind site was expected as this is the calibration point in the LIDAR PM retrieval algorithm and both are converted to PM_k through the same MCF_k. The downwind sites, however, were not used as direct calibration points, and thus may exhibit greater differences between LIDAR and OPC period-averaged values. On a side note, the proximity of all upwind OPC and LIDAR PM_k demonstrates the selected time interval between LIDAR calibration stares was sufficient to adequately characterize
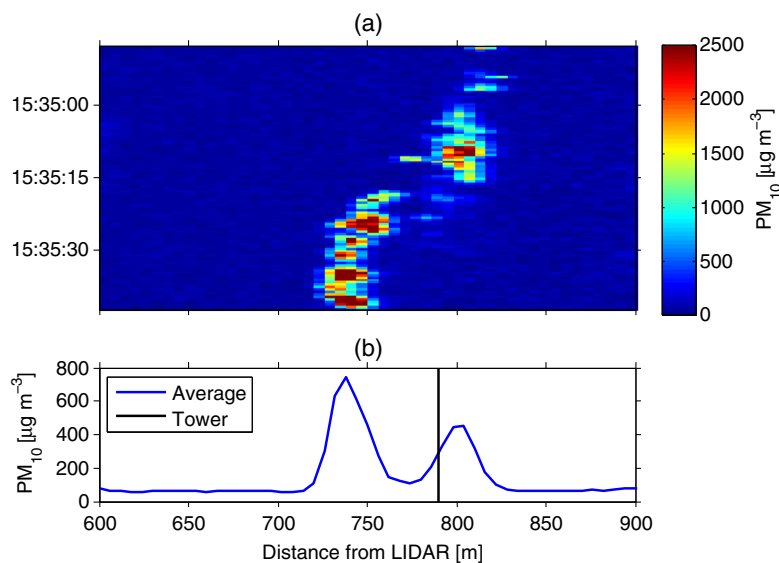

Fig. 6 (a) LIDAR-derived PM_{10} in a time versus distance from the LIDAR concentration map and (b) a time series average concentration versus distance from the LIDAR graph. Data were collected in a stare past the downwind tower during the June 18 sample period.
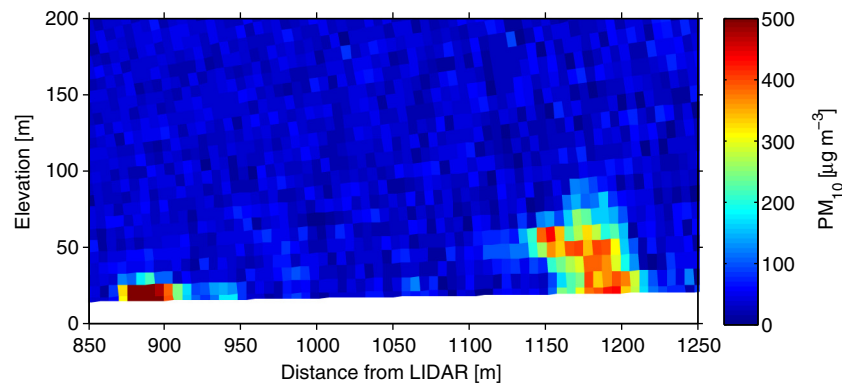
Fig. 7 Image of plumes in a vertical LIDAR scan on June 5.

changes in upwind PM. It also supports the assumption made in the flux calculations that upwind PM_k is relatively constant.

Differences in calculated PM_k between instruments may result from a variety of factors, including but not limited to the following: sample volume differences ($OPCs - 1 \ L \cdot min^{-1}$; $MiniVols - 5 \ L \cdot min^{-1}$; LIDAR $- 6 \ m$ bin length $x \sim 1 \ m$ beam diameter sampled at 10 kHz with data averaged over 0.5 s); sampling frequency at the point sensor location (MiniVol and OPC–continuous; LIDAR–upwind: 3 to 5 min per 15 min, and downwind: 1 to 3 min per 15 min); LIDAR sample timing with respect to plume location (i.e., simultaneous presence of both the LIDAR beam and a transient plume impacting the instrumented tower versus the total time the plumes impacted the tower); and the differences between the MCF_k values calculated at the comparison site and the average MCF_k across all measurement sites used to convert V_k to PM_k. LIDAR stare time used in the comparison with continuously running, stationary OPCs, and MiniVols was limited by the need to perform vertical scans for flux estimation. Better agreement is expected on the downwind side with an increasing proportion of time spent adjacent to downwind samplers.

The error introduced in this inter-instrument comparison associated with using a spatially averaged MCF_k was generally less than $\pm30\%$ during this study based on the 95% confidence intervals (CIs) reported in Table 3. Large differences in $PM_{2.5}$ between the filter- and optical-based methods were observed across all sample periods due to the use of a constant $MCF_{2.5}$ value that was not derived from onsite PM measurements. However, OPC and LIDAR $PM_{2.5}$ levels were close.

An example of an inter-instrument comparison is provided in Table 5 for the June 18 sample period, the period shown in Fig. 5. In this instance, average upwind OPC and LIDAR PM_{10} and TSP concentrations were within 15% and 7%, respectively, of the values reported by the MiniVol. Downwind LIDAR PM_{10} and TSP values were 73% and 64% of OPC levels, respectively, while the OPC PM_{10} was 6% higher than the PM_{10} concentration from the filter sample. The differences at the downwind location were likely caused, in large part, by the relatively small amount of time the LIDAR sampled adjacent to the point sensors. Longer stare periods at downwind locations are expected to yield better PM_k accuracy and are planned for future deployments.

3.2 Estimated Emissions and Control Efficiencies

The PM_k data from the LIDAR, OPCs, and MiniVols were all used to calculate PM emissions using mass balance and inverse modeling techniques. Table 6 provides the results of these calculations, as well as the summed emissions from each tillage management practice. Stated uncertainties are the 95% CIs about the average and have been provided for cases where $n \geq 3$.

The summed conservation tillage sequence emissions (E_{ST}) consist of the following three passes: strip–till, plant, and herbicide application. The LIDAR did not detect plumes in downwind vertical scans during the herbicide application, as indicated by the no plumes observed designation. However, downwind PM samplers reported small increases in concentrations

Table 5 Comparison of period average PM mass concentrations as reported by collocated MiniVol filter samplers and OPCs, as well as the adjacent LIDAR bin, at measurement heights of 9 m agl at upwind and downwind tower locations for the June 18 sample period. Error values provided for OPC and LIDAR PM_k represent the 95% confidence interval (CI).

	$PM_{2.5}$ ($\mu g \cdot m^{-3}$)	PM_{10} ($\mu g \cdot m^{-3}$)	TSP ($\mu g \cdot m^{-3}$)
	Upwind		
MiniVol PM sampler	30.1	56.5	195.4
OPC $\pm$ 95% CI	4.9 $\pm$ 0.1	48.2 $\pm$ 1.1	185.4 $\pm$ 8.5
LIDAR $\pm$ 95% CI	5.1 $\pm$ 0.1	50.8 $\pm$ 1.3	200.0 $\pm$ 6.7
	Downwind		
MiniVol PM sampler	63.2	87.5	—
OPC $\pm$ 95% CI	6.4 $\pm$ 0.5	93.0 $\pm$ 15.1	442.3 $\pm$ 95.2
LIDAR $\pm$ 95% CI	6.3 $\pm$ 0.1	68.1 $\pm$ 2.1	284.5 $\pm$ 10.2

over background levels during this sample period, leading to small EFs relative to the other operations investigated. The herbicide application operation was performed by a small tractor pulling a spray applicator; as no subsurface disturbance occurred, the only active PM sources were the tractor and implement tires and the spray droplets.

The summed emissions for the conventional tillage method (E_{CT}) include the following 13 passes in order: two break down in-field border passes, chisel, two disk passes, lister, two cultivator passes, roll, plant, fertilizer injection, and two more cultivator passes. The EFs for the break down in-field borders operation have been distributed over the entire field area (10.1 ha) instead of just the area worked (1.0 ha) to represent the emissions over the entire field in the E_{CT} calculation. As the LIDAR system was unavailable to take measurements during the last sample period for the third cultivator pass, the emissions of the last two cultivator passes were assumed to be equal to the observed emissions for the first two cultivator passes. The inverse modeling method found that the third cultivator pass emitted from 0.6 to 3.6 times as much PM as calculated for the first and second cultivator passes, with an average of 2.1.

Some of the LIDAR-derived EFs were much higher than those calculated by inverse modeling within an operation and PM size fraction, particularly for the chisel, disk 1, and lister passes. Others were not statistically different due to overlapping CIs. E_{CT} and E_{ST} EFs from the LIDAR dataset were significantly higher, based on the CIs, than those calculated through inverse modeling in all cases but the $PM_{2.5}$ E_{ST}. The LIDAR- and OPC-based $PM_{2.5}$ EFs were smaller than the MiniVol-based $PM_{2.5}$ EFs in all cases, which is likely to be related to the use of the average soil density as the $MCF_{2.5}$ in place of calculated values as discussed earlier.

While the EFs from published studies are generally not in close agreement, a high range of variability is expected from measurements made under different meteorological and soil conditions, as demonstrated in Ref. 5. Some of the PM_{10} EF values calculated from this study were in agreement with those given by Refs. 5 and 10, such as the cultivate, roll, strip–till, conventional tillage planting, and conservation tillage planting passes. Other EFs were much larger than values previously reported, especially the disk 1, disk 2, chisel, and lister passes. The results from this campaign were, in general, not in as good agreement as previous studies have been.

The η values were also included in Table 6. They were calculated using the following equation based on a collection efficiency equation found in Ref. 31 and represents the PM emissions reduction of the conservation tillage compared to the conventional tillage:

$$\eta = \frac{E_{CT} - E_{ST}}{E_{CT}}. \qquad (5)$$

The strip–till conservation tillage reduced PM emissions in all size fractions by about 90%. The reduction in total tractor operation time per unit area of field was similar to PM reductions at

Table 6 Average particulate matter (PM) emission factors (EFs) and 95% confidence intervals (CI) estimated for the conventional and conservation tillage management practices. Emissions were calculated through applying a mass balance technique to mass-calibrated LIDAR data and inverse modeling with AERMOD and both filter-based particle sampler (MiniVol) and mass-calibrated OPC data. Control efficiency (η) results are also provided for the conservation tillage management practice. NPO = no plumes observed.

| | Average emission factors $\pm$ 95% CI (mg $\cdot$ m^{-2}) | | | | | | | | |
| | PM$_{2.5}$ | | | PM$_{10}$ | | | TSP | | |
	LIDAR	OPC	MiniVol	LIDAR	OPC	MiniVol	LIDAR	OPC	MiniVol
Conservation tillage method									
Strip–till	26.9 ± 6.1	14.5 ± 3.0	35.7 ± 6.1	523.8 ± 117.8	452.5 ± 85.7	315.6 ± 86.9	4450.5 ± 1000.9	2180.4 ± 583.6	1652.9 ± 881.6
Plant	50.2 ± 15.0	6.6 ± 3.3	133.5	175.6 ± 52.6	173.5 ± 36.8	123.3	567.6 ± 169.9	881.8 ± 234.5	857.4 ± 523.2
Herbicide application	NPO	0.7 ± 0.4	44.0	NPO	40.9 ± 12.7	64.3	NPO	114.8 ± 55.9	133.7 ± 71.9
Sum, E$_{ST}$	**77.1 ± 16.2**	**21.8 ± 4.5**	**213.2**	**699.4 ± 129.0**	**666.9 ± 94.1**	**503.2**	**5018.1 ± 1,015.2**	**3177.0 ± 631.5**	**2644.0 ± 1,027.7**
Conventional tillage method									
Break down in-field borders	3.0 ± 1.8	0.7 ± 0.1	—	33.6 ± 20.8	51.2 ± 7.9	—	152.3 ± 94.4	617.6 ± 79.8	5.8
Chisel	101.1 ± 11.1	18.3 ± 5.4	—	1132.8 ± 123.9	647.4 ± 181.0	—	4997.9 ± 546.8	3828.2 ± 758.5	—
Disk 1	210.1 ± 49.3	37.0 ± 9.4	—	3,410.7 ± 799.9	1452.5 ± 161.9	—	17,440.2 ± 4,090.4	9693.3 ± 744.5	—
Disk 2	58.9 ± 16.2	36.4 ± 13.3	—	1066.4 ± 293.2	1797.5 ± 703.1	—	6023.4 ± 1,655.8	10,483.4 ± 2976.9	—
Lister	302.8 ± 127.5	19.4 ± 2.9	—	4608.1 ± 1940.8	849.5 ± 150.5	—	23,375.6 ± 9,845.2	4918.9 ± 1,169.8	—
Break down ditches, cultivator passes 1 and 2, and roller	22.9 ± 4.5	7.8 ± 5.0	52.7 ± 19.8	109.4 ± 21.3	137.1 ± 65.5	107.9 ± 47.7	354.0 ± 69.0	687.1 ± 443.8	—
Plant	8.3 ± 2.1	6.4 ± 4.1	86.4	79.5 ± 20.2	170.7 ± 81.3	87.6	285.3 ± 72.4	910.4 ± 487.1	495.1
Fertilizer injection	9.4 ± 6.2	21.5 ± 17.6	67.1 ± 63.1	139.4 ± 91.9	642.5 ± 380.3	515.9	684.1 ± 451.3	4602.1 ± 2370.2	3686.7
Cultivator passes 3 and 4	—	11.1 ± 4.0	31.9 ± 4.1	—	369.8 ± 157.7	234.5	—	2459.4 ± 894.9	2063.5 ± 436.7
Sum, E$_{CT}$	**811.1 ± 138.7**	**186.2 ± 27.0**	**—**	**11,051.2 ± 2,126.0**	**6813.4 ± 888.8**	**—**	**54,881.3 ± 10,814.4**	**42,651.5 ± 4406.9**	**—**
CMP control effectiveness									
η, %	90.5	88.3	—	93.7	90.2	—	90.9	92.6	—

The bold values represent the sum of the emissions (E$_{ST}$ and E$_{CT}$).

84% (see Table 1). The η results had a small range of <6% across methodologies and size fractions, despite large differences in summed emissions between methodologies.

Limitations of the PM sensors and AERMOD contribute to limitations and uncertainties in the estimated EFs. For instance, the scanning LIDAR system did not collect data below about 10 m agl at the range of the fields due to eye-safety concerns, which results in portions of plumes not being sampled and included in EF estimates. Vice versa, the inability to locate point sensors above 10 m limits their ability to characterize the plume depth. In this case, the LIDAR and point sensors complement each other in mapping the emitted plumes, as previously demonstrated by Ref. 6. In addition, measurements at a few points may or may not represent the plume characteristics sufficiently to accurately determine the EF, particularly for a roving source such as in agricultural tillage. This was mitigated by deploying as many samplers at different sites within the downwind plume as possible. Another limitation that was identified by Ref. 11 and was also present in this analysis is AERMOD's poor simulation of elevated plumes from agricultural tillage, particularly plumes completely detached from the ground.

4 Conclusions

A study was conducted in California's San Joaquin Valley to estimate the PM_k emissions η of a CMP relative to the conventional tillage practices. PM_k concentrations resulting from a spring tillage sequence transitioning from a winter wheat silage crop to a summer corn crop were monitored. The strip–till conservation tillage CMP, consisting of three operations in three passes, was compared against the conventional tillage sequence, consisting of nine operations in 13 passes. The CMP reduced the amount of tractor operation time per unit area by 84%. Emissions were estimated through inverse modeling with point sensor PM_k and through a mass balance applied to mass-calibrated LIDAR PM_k.

A significant portion of the filter-based samples was rendered unusable for emissions calculations due to sampling irregularities and errors. The incompleteness of this PM_k dataset prevented the calculation of total EFs per management practice and the CMP η. However, the OPC- and LIDAR-based PM_k and EF datasets were sufficiently complete to calculate η values, which were all about 90%. Some of the calculated EFs were within the range found in the literature, but others were significantly higher. The total emissions per management practice and PM size fraction varied significantly, based on the 95% CIs, between the measurement and emissions estimation methodology combinations. This study demonstrated that the strip–till CMP can significantly reduce PM emissions and tractor operation time during the investigated spring tillage sequence.

References

1. C. I. Davidson, R. F. Phalen, and P. A. Solomon, "Airborne particulate matter and human health: a review," *Aerosol Sci. Technol.* **39**, 737–749 (2005).
2. Environmental Protection Agency (EPA), "Designations and classifications for initial PM-10 nonattainment areas," *Fed. Reg.* **56**(51), 11101–11105 (1991).

3. EPA, "Reclassification of moderate PM-10 nonattainment areas to serious area," *Fed. Reg.* **58**(5), 3334–3342 (1993).

4. San Joaquin Valley Air Pollution Control District (SJVAPCD), "Conservation management practices program report," San Joaquin Valley Air Pollution Control District, 2006, http://www.valleyair.org/farmpermits/updates/cmp_program_report_for_2005.pdf (8 May 2013).

5. R. G. Flocchini et al., "Interim report: sources and sinks of PM10 in the San Joaquin Valley," (Crocker Nuclear Laboratory, UC-Davis, California 2001), http://www.arb.ca.gov/research/apr/reports/l2022.pdf.

6. B. A. Holmén, W. E. Eichinger, and R. G. Flocchini, "Application of elastic LIDAR to PM10 emissions from agricultural nonpoint sources," *Environ. Sci. Technol.* **32**, 3068–3076 (1998).

7. B. A. Holmén et al., "LIDAR-assisted measurement of PM10 emissions from agricultural tilling in California's San Joaquin Valley–Part I. LIDAR," *Atmos. Environ.* **35**, 3251–2364 (2001).

8. B. A. Holmén et al., "LIDAR-assisted measurement of PM10 emissions from agricultural tilling in California's San Joaquin Valley–Part II: emission factors," *Atmos. Environ.* **35**, 3265–3277 (2001).

9. J. Kasumba et al., "Agricultural PM10 emissions from cotton field disking in Las Cruces, NM," *Atmos. Environ.* **45**, 1668–1674 (2011).

10. N. M. Madden, R. J. Southard, and J. P. Mitchell, "Conservation tillage reduces PM10 emissions in dairy forage rotations," *Atmos. Environ.* **42**, 3795–3808 (2008).

11. K. D. Moore et al., "Particulate emissions calculations from fall tillage operations using point and remote sensors," *J. Environ. Qual.* **42**, 1029–1038 (2013).

12. J. Wang et al., "Local dust emission factors for agricultural tilling operations," *Soil Sci.* **175**, 194–200 (2010).

13. California Air Resources Board (ARB), "Area source methods manual, section 7.4: agricultural land preparation," California ARB (2003), www.arb.ca.gov/ei/areasrc/fullpdf/full7-4.pdf (7 November 2011).

14. California ARB, "Area source methods manual, section 7.5: agricultural harvest operations," California ARB (2003), www.arb.ca.gov/ei/areasrc/fullpdf/full7-5.pdf (7 November 2011).

15. D. Williams et al., "Atmospheric LiDAR coupled with point measurement air quality samplers to measure fine particulate matter (PM) emissions from agricultural operations, Part 2 of the California 2007-2008 tillage campaigns: spring 2008 data analysis," Report EPA/600/R-14/191, (EPA, Washington, DC 2014).

16. U.S. Department of Agriculture, "Natural resources conservation service (USDA NRCS)," *Web Soil Survey 2.0.*, 2009, http://websoilsurvey.nrcs.usda.gov/app/ (2 January 2009).

17. J. W. Doran and A. Jones, *Methods for Assessing Soil Quality*, SSSA Special Publication Number 49, Soil Science Society of America, Madison, Wisconsin (1996).

18. J. S. Hill, P. D. Patel, and J. R. Turner, "Performance characterization of the MiniVol PM2.5 Sampler," presented at *Air and Waste Management Association's 92nd Annual Meeting, Pittsburgh, Pennsylvania, Paper 99-617*, June 20–24, Air and Waste Management Association (1999).

19. J. C. Chow et al., "PM2.5 and PM10 mass measurements in California's San Joaquin Valley," *Aerosol Sci. Technol.* **40**(10), 796–810 (2006).

20. F.-L. Chen et al., "Coarse particulate matter concentrations from residential outdoor sites associated with the North Carolina asthma and children's environment studies (NC-ACES)," *Atmos. Environ.* **41**, 1200–1208 (2007).

21. K. D. Moore et al., "Derivation and use of simple relationships between aerodynamic and optical particle measurements," *J. Environ. Eng.* **141**(4), 04014078 (2015).

22. C. C. Marchant et al., "Aglite LIDAR: a portable elastic LIDAR system for investigating aerosol and wind motions at or around agricultural production facilities," *J. Appl. Remote Sens.* **3**(1), 033511 (2009).

23. V. V. Zavyalov et al., "Aglite LIDAR: calibration and retrievals of well characterized aerosols from agricultural operations using a three-wavelength elastic LIDAR," *J. Appl. Remote Sens.* **3**(1), 033522 (2009).

24. C. Marchant, "Algorithm development of the AGLITE-LIDAR instrument," MS Thesis, Utah State University (2008).

25. A. S. Jursa, *Handbook of Geophysics and the Space Environment*, Hanscom Air Force Base, NTIS, Massachusetts (1985).

26. J. D. Klett, "LIDAR inversion with variable backscatter/extinction ratio," *Appl. Opt.* **24**, 1638–1643.

27. A. J. Cimorelli et al., "AERMOD: a dispersion model for industrial source applications. Part I: general model formulation and boundary layer characterization," *J. Appl. Meteorol.* **44**, 682–693 (2005).

28. EPA., "AERSURFACE User's Guide," Report EPA-454/B-08-001, EPA Office of Air Quality Planning and Standards, Research Triangle Park, North Carolina (2008).

29. S. P. Arya, *Air Pollution Meteorology and Dispersion*, Oxford University Press, New York (1998).

30. G. E. Bingham et al., "LIDAR based emissions measurement at the whole facility scale: method and error analysis," *J. Appl. Remote Sens.* **3**(1), 033510 (2009).

31. D. C. Cooper and F. C. Alley, *Air Pollution Control: A Design Approach*, Waveland Press Inc., Prospect Heights, Illinois (2002).

32. USDA NRCS, "National soil survey handbook, title 430-VI," http://soils.usda.gov/technical/handbook/ (2007).

Kori D. Moore is an environmental engineer at the Space Dynamics Laboratory, Utah State University Research Foundation, and a PhD candidate at Utah State University. He received his BS and MS degrees in civil and environmental engineering from Utah State University in 2007. His current research interests include air-pollution emissions from agriculture, winter-time air-pollution episodes, and air-quality modeling.

Michael D. Wojcik is a senior scientist at the Space Dynamics Laboratory, Utah State University Research Foundation. He received his BS degree in chemistry in 1996 from Rensselaer Polytechnic Institute and his PhD in physical chemistry from the University of Idaho in 2002. His current research interests include remote sensing of wind and aerosols and trace level detection of atmospheric gas species using molecular laser spectroscopy.

Randal S. Martin is an associate research professor in the Department of Civil and Environmental Engineering, Utah State University, and holds a joint appointment at the Utah Water Research Laboratory. He received his BS degree in environmental engineering from Montana Tech in 1982 and his MS and PhD degrees in civil and environmental engineering from Washington State University in 1989 and 1992. His research interests include behaviors of ambient particulate matter and ozone.

Christian C. Marchant is currently an image scientist at the National Geospatial-Intelligence Agency and formerly was a graduate research assistant at Space Dynamics Laboratory, Utah State University Research Foundation. He received his BS degree in electrical engineering from Brigham Young University in 2004 and his MS and PhD degrees in electrical engineering from Utah State University in 2008 and 2010, respectively. He was a space scholar intern with the Air Force Research Laboratory in summer 2009.

Derek S. Jones is an applications engineer at Campbell Scientific, Inc. and formerly was a graduate research assistant at the Space Dynamics Laboratory, Utah State University Research Foundation. He received his BS degree in mathematics in 2004 and his MS degree in civil and environmental engineering in 2009 from Utah State University. His current research interests include instrumentation and experimental design.

William J. Bradford is an applications engineer at Campbell Scientific, Inc. and formerly was an environmental engineer at the Space Dynamics Laboratory, Utah State University Research Foundation. He received his BS degree in civil and environmental engineering from Utah State University in 1997. Currently, he provides technical support to researchers and engineers that utilize Campbell Scientific data loggers and sensors in the fields of geotechnical and structural engineering.

Gail E. Bingham is a chief scientist at the Space Dynamics Laboratory, Utah State University Research Foundation. He received his BS degree in biometeorology from Utah State University in 1968 and his MS and PhD degrees in micrometeorology from Cornell University in 1971 and 1972, respectively. His current research interests include microgravity plant growth and development, environment science, and space sensor design and engineering.

Richard L. Pfeiffer is a chemist at the National Laboratory for Agriculture and the Environment, Agricultural Research Service, U.S. Department of Agriculture. He received his BS degree in chemistry from the University of South Dakota in 1978, and his PhD in veterinary medical sciences from the University of Illinois in 1986. He has authored more than 30 journal papers and written several book chapters. His current research deals with advanced instrumentation for the measurement of greenhouse gases.

John H. Prueger is a soil scientist at the National Laboratory for Agriculture and the Environment, Agricultural Research Service, U.S. Department of Agriculture. He received his PhD in micrometeorology from Utah State University in 1991. He is the author of more than 100 journal papers and has written 10 book chapters. His current research interests include turbulence exchange processes at the boundary-layer (surface atmosphere) and scaling issues for processes occurring at the surface to regional scale landscapes.

Jerry L. Hatfield is a laboratory director at the National Laboratory for Agriculture and the Environment, Agricultural Research Service, U.S. Department of Agriculture. He received his PhD in agricultural climatology from Iowa State University in 1975. He is the author of more than 414 journal papers and has written 82 book chapters and edited 16 books. His current research interests include quantifying the interactions among soil-plant-atmosphere components and the impact of agricultural systems on environmental quality.